

Design of a Digital Servo Control IC for Permanent Magnet Synchronous Motors with Linear Hall Sensors

Yen-Chuan Chang and Ying-Yu Tzou, *Member, IEEE*

Power Electronics Systems & Chips Lab.
Advanced Power Electronics Center
Department of Electrical and Control Engineering
National Chiao Tung University, Taiwan.

Abstract—This paper presents the design and architecture implementation of a digital position control IC for permanent magnet synchronous motors (PMSMs) with sinusoidal flux distribution using linear Hall sensors for low-cost motion control applications. The absolute rotor position is calculated from the measured Hall sensor signals and a speed estimator is devised to generate speed feedback for the servo loop compensator. The developed digital servo control IC for PMSM motors with linear Hall sensors consists of three major control blocks: a servo loop controller, a position and speed estimator, and a field-oriented torque controller. The accuracy of positioning control resolution can be improved by a position error compensation table via external position calibration. All the control blocks are realized by using digital circuitry with configurable and reusable intellectual property (IP) blocks. Experiment results are presented to verify the performance and feasibility of the proposed IC.

Index Terms—digital ac servo IC, permanent magnet synchronous motor, linear Hall sensor, position calculator, speed estimator, position calibration, digital torque control.

I. INTRODUCTION

Small motors (below 3 Watts) have been widely employed in today's consumer electronics for speed or position control applications, such as cooling fans, DVD spindle drives, digital cameras, image scanners, and electronics toys. Requirements in control and energy saving performances of small motors become more stringent in company with size reduction. A very tight cost constraint imposes on the feasible solution for the control of small motors. Most conventional approaches in design control ICs for small motors are using analog technology with only limited functions. Advantages in adopting analog technology mainly resides on cost considerations, however, suffers with limited functions and applications. Owing to the rapid progress in motor control and microelectronics technologies, development in software servo and motor control IC will become a major trend [1]-[3]. Although most ac drives (ac servo drives or universal PWM inverters) in use today adopt microprocessor-based digital control strategy, the implementation of current control loop and PWM control

This work was supported by the National Science Council, Taipei, Taiwan, R.O.C. Project no. NSC 95-2221-E-009-338-MY3.

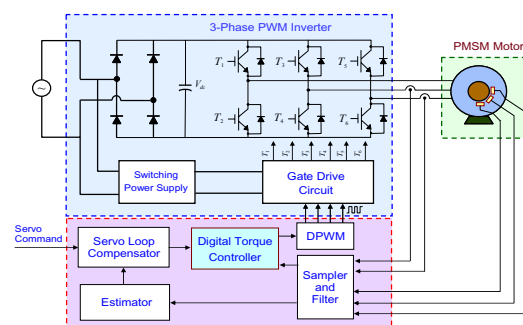


Fig. 1. Block diagram of a servo control system for PMSM.

are still tied to analog control circuitry. This kind of control scheme possesses the advantage of fast dynamic response, but suffers the disadvantages of complex circuitry, limited functions, and difficulty in circuit modification.

The rapid development in high-performance, low-cost DSP/FPGA has encouraged research on low-cost digital servo control IC for small brushless dc motor for low-resolution position control. This digital control scheme has the advantages of simple circuitry, software control, and flexibility in adaptation to various applications [4]-[5]. However, generating PWM gating signals and current control loops require a high sampling rate to achieve a wide bandwidth performance [6]-[7]. Mixed-mode technology has been employed in design of today's motor control ICs. However, most of the commercial control ICs are still fixed in structure and unable to be programmed. Programmability becomes important in modern motor control ICs in many applications.

This paper presents the design of a programmable digital servo control IC for PMSMs with linear Hall sensors. Fig. 1 shows the block diagram of a PMSM servo control system using the proposed control IC. By using the hierarchical and modular realization strategy, every block in FPGA is designed toward a specific function of control law, and has its own registers which can be configured by users to build up a control system according to different applications. The proposed implementation architecture has been realized using a single-chip FPGA controller. Unlike traditional DSP or microcontrollers, users do not need to design software

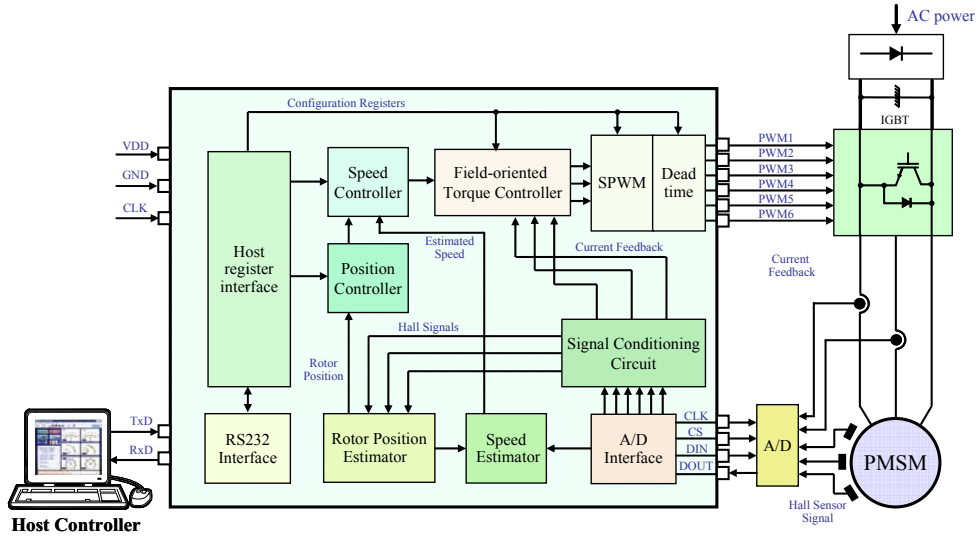


Fig. 2. The internal architecture of the digital servo control IC.

programs to develop control algorithms. Therefore, it provides a simple low-cost and fast time-to-market solution for the servo control of permanent magnet brushless motors with linear Hall sensors.

II. SERVO CONTROL SYSTEM DESIGN

A. System Configuration

Fig. 2 shows the internal architecture of the proposed digital servo control IC for permanent magnet synchronous motor. The servo control IC consists of a three-phase PWM generator with a programmable deadtime generator, a field-oriented torque controller, a velocity loop controller, a position loop controller, a position estimator based on the feedback signals from linear Hall sensors, and speed estimator based on the estimated position. In most servo control systems, the position information is obtained from encoders or resolvers, which are costly and usually need a special installation of the sensing device for the machine. Linear Hall effect sensors conventional used for the commutation control and current reference for PMSM motor control and also be used to provide positioning and velocity feedback information via signal processing techniques.

Fig. 3 shows two control schemes for brushless dc motor with sinusoidal flux distribution. The first control method is based on encoder feedback which guarantees high performances and better position tracking capability. The second one is usually adopted in low cost drives, where a certain reduction in control accuracy can be tolerated [8]. In this IC, we employ the second method based on current multiplier control to decrease the price in building a servo control system.

The linear Hall effect sensors produce an output signal which is proportional to the intensity of the induced field by the permanent magnet. For a sinusoidal brushless ac motor, the Hall effect sensors, which are displaced 120 electrical degrees from each other, can generate three sinusoidal

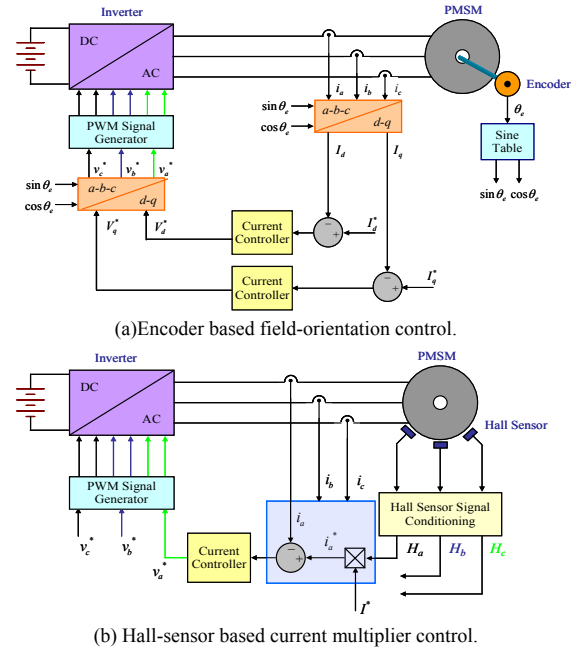


Fig. 3. Control schemes for brushless dc motor with sinusoidal flux distribution.

signals that are exactly in phase with back-EMF. The signals are regarded as a unit amplitude reference for the corresponding phase current. The torque command generated from the speed controller is multiplied by the reference Hall sensor signals to produce phase current command. In this way, the field-oriented torque control is achieved by generating current references in the three-phase stationary frame without the stationary-to-rotating reference frame transformation and its inverse.

The control IC is synthesized using modular circuit design methodology. Every block is designed toward a specific function and there are a lot of control registers in the

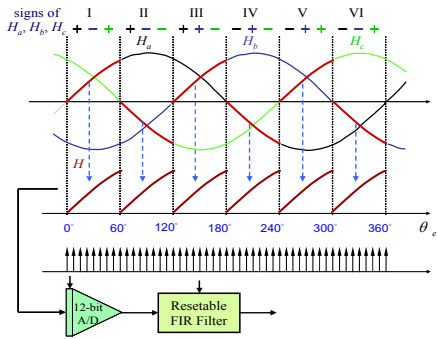


Fig. 4. Output waveforms of the linear Hall sensors and sampling mechanism.

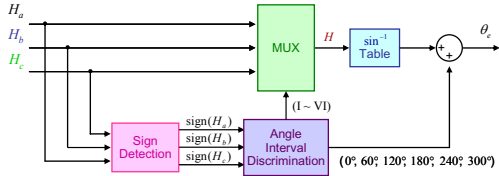


Fig. 5. Position detection mechanism.

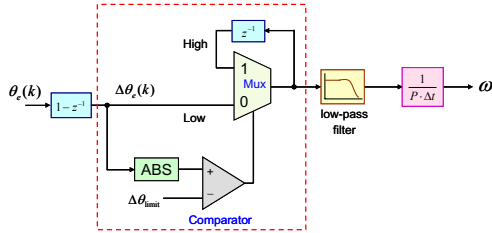


Fig. 6. Block diagram of the speed estimator.

different function blocks. System constructors can set the registers according to different applications. To simplify the interface circuit and increase the practicality of the IC, the registers in the control IC is configured by a Graphical User Interfaces (GUI) program in Matlab on PC. Therefore, it takes little effort building up a servo system, and provides a flexible and fast time-to-market solution for PMSM motor drives with linear Hall effect sensors.

B. Position and Speed Estimation with Linear Hall sensor

Fig. 4 shows the ideal output waveforms of the linear Hall sensors and the sampling mechanism. A nonlinear compensator is used to rescale the measured rotor position signal and a weighted FIR filter is used to remove the measured noises from Hall sensors and signal conditioning circuit. The 360 electrical degrees is divided into six intervals and each of them is 60 electrical degrees. The rotor position is first distinguished into the six intervals by the sign of three Hall sensor signals H_a , H_b and H_c . Second, a fine discrimination is made by an arcsine table look-up from H_a , $-H_c$, H_b , $-H_a$, H_c and $-H_b$ according to the six intervals. Fig. 5 shows the position detection mechanism from a series of measured rotor positional signals.

Fig. 6 shows the block diagram of the speed estimator based on the increment feedback from the calculated rotor

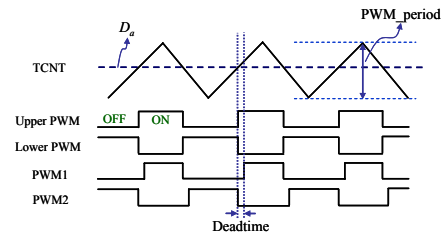


Fig. 7. Timing diagram of the PWM generator.

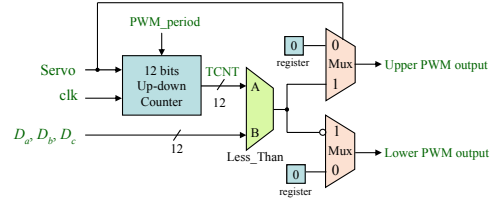


Fig. 8. Hardware circuit of the PWM generator.

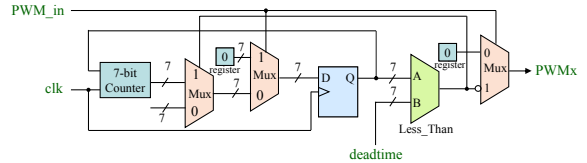


Fig. 9. Hardware circuit of the deadtime generator.

position. $\theta_e(k)$ is the estimated rotor position, $\Delta\theta_e(k)$ is the incremental position value in one sampling period and ω is the estimated speed. To prevent the estimated error occurs when the rotor position changes from 0 to 360 electrical degrees or 360 to 0 electrical degrees, the incremental position is replaced by the value in the previous sampling period when the estimated incremental value is larger than the preset limit $\Delta\theta_{limit}$.

III. DETAILED DESCRIPTION OF THE FUNCTIONAL BLOCKS

A. PWM Generator

A 12-bit digital three-phase complementary PWM generator with configurable PWM frequency and deadtime is implemented in the control IC. This realization scheme has the advantage of simple hardware design compared with the asymmetrical PWM scheme and the harmonic spectrum has little effect with a high switching frequency for small motor applications. The digital current loop sampling and modulation scheme can be doubled by using asymmetrical PWM scheme since the comparator updates twice in one switching period. Fig. 7 shows the timing diagram of the PWM generator. Three compare registers D_a , D_b and D_c are used to hold the modulating values, and they are constantly compared with the value of the timer counter TCNT. In this way, the output pulse is generated whose on (or off) duration is proportional to the value in the compare registers. The PWM frequency can be determined by the maximum value of TCNT counter and system clock frequency as:

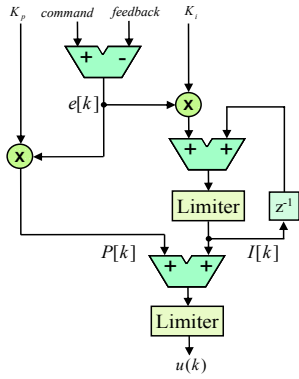


Fig. 10. Hardware structure of the PI controller.

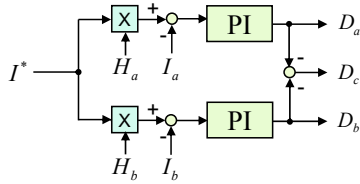


Fig. 11. Block diagram of the current control loop.

$$f_{PWM} = \frac{f_{clk}}{N \times 2} \quad (1)$$

where f_{clk} is the system clock and N is the maximum value of the counter TCNT. Fig. 8 shows the hardware circuit of the digital PWM generator.

The semiconductor devices used as power switches are not ideal, so they react with a certain delay to the driving signals corresponding to turn-on and turn-off. To avoid short-circuit in any leg of the power inverter, the deadtime should be inserted when a switch is turning on. A 7-bit deadtime generator is implemented, and for a 40 MHz system clock, it can generate a time delay from 0 to 3.2 μ s. Fig. 9 shows the hardware circuit of the deadtime generator.

B. Servo Loop Controller

The servo loop consists of a speed controller and a position controller, and both of them are regulated by the digital PI control law, which is formulated as

$$u[k] = P[k] + I[k] \quad (2)$$

where the proportional term is

$$P[k] = K_p \cdot e(k) \quad (3)$$

and the integral term is

$$I[k] = K_i \cdot e(k) + I[k-1] \quad (4)$$

where the error term $e[k]$ is the difference between the command and feedback signals, and K_p , K_i are the proportional and integral gain, respectively.

Fig. 10 shows the hardware structure of the PI controller. In order to reduce the whole chip size, a scheduling strategy for realizing the PI controller by using finite-state-machine is used. Only one multiplier and one adder are required to execute the PI control. The bit length of the PI controller is

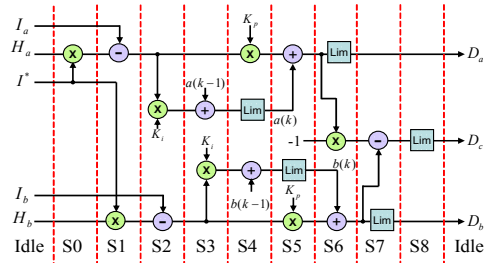


Fig. 12. The computation steps of the current control loop.

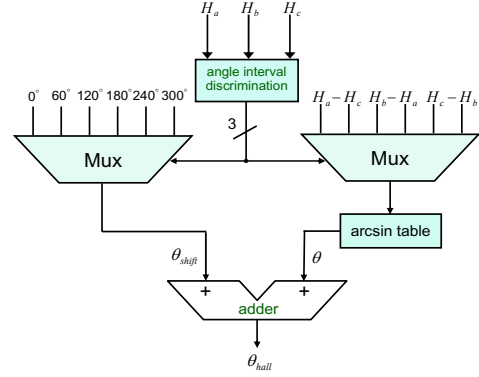


Fig. 13. Hardware structure of the position estimator.

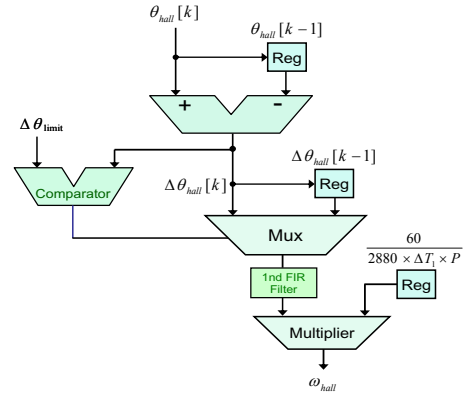


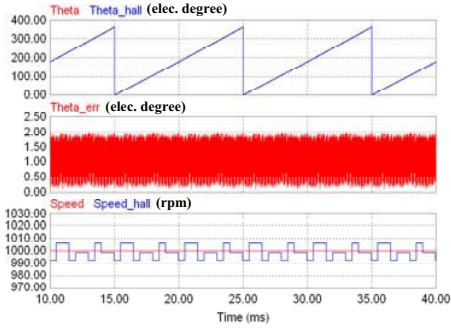
Fig. 14. Hardware structure of the speed estimator.

16-bit, and K_p , K_i are in Q-10 format. There are two saturation limiters in Fig. 10. The anti-windup limit at the output of the integrator is to prevent unwanted overshoot caused by the inertial property of the integrator. The output limit of the PI regulator limits the maximum output command.

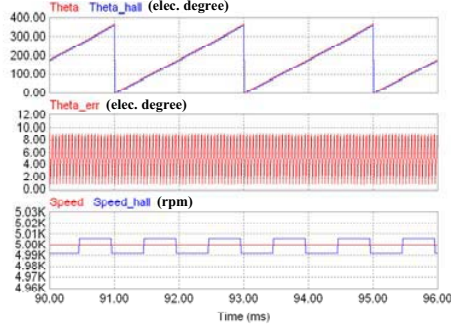
C. Field-oriented Torque Controller

Fig. 11 shows the block diagram of field-oriented torque control loop with PI controller. The phase current should be aligned in phase with the back-EMF waveforms so as to achieve high torque/current ratio. The current command I^* from speed controller is first multiplied by H_a and H_b , then the PI controller is used to generate the duty D_a , D_b and D_c , which will be sent to the PWM generator.

In order to reduce the whole chip size, a scheduling strategy for realizing the field-oriented torque control is



(a)



(b)

Fig. 15. Simulation result with ideal Hall sensor signals under (a) 1000 rpm and (b) 5000 rpm operation.

implemented by using finite-state-machine. Only one multiplier and one adder are required to execute the PI control law as shown in Fig. 12.

D. Position and Speed Estimator

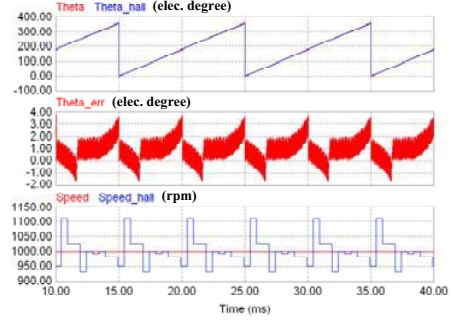
Fig. 13 shows the hardware structure of the position estimator with linear Hall sensor signals. The Hall signals are converted from a 12-bit AD converter, and the least two significant bits are truncate to reduce the influence of noise, then the value of Hall signals are from -512 to 511. To estimate the rotor position, a coarse discrimination is made by the sign of the Hall signals, and then a fine discrimination in 0 to 60 electrical degrees is made by a look-up table to estimate the rotor position. A sine-table with 433 points is needed, which is obtained from

$$512 \times \sin 60^\circ \approx 443. \quad (5)$$

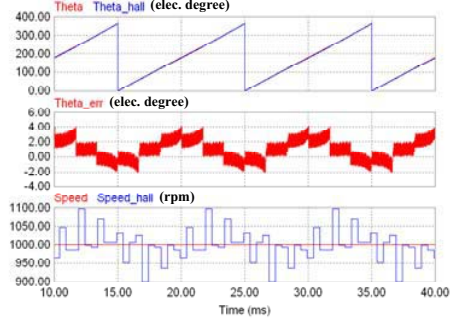
The rotor position in the look-up table is in Q-3 format. The speed is then estimated from

$$\omega_{hall}[k] = \frac{\theta_{hall}[k] - \theta_{hall}[k-1]}{2880 \times \Delta T_1} \times \frac{60}{P} \quad (6)$$

where ω_{hall} is the estimated speed in rpm, θ_{hall} is the estimated position in Q-3 format, ΔT_1 is the sampling time of speed calculation and P is the number of pole pairs. In (6), the recognizable lowest speed is associated with the sampling time. For a motor with six pole pairs, the lowest calculated speed is 6.944 rpm with 2 kHz sampling time. Fig. 14 shows the hardware structure of the speed estimator.



(a)



(b)

Fig. 16. Simulation result with non-ideal Hall sensor signals under 1000 rpm (a) with amplitude 102% on H_a , 98% on H_b , and (b) with offset 2% on H_a , -2% on H_b .

To verify the position and speed estimator design in VHDL, a co-simulation with Matlab, PSIM and Modelsim is applied. A motor drive system is constructed in Matlab by linking PSIM and Modelsim. Fig. 15(a) and (b) shows the simulation result under constant 1000 and 5000 rpm operation, and the sampling time of the position estimator and the speed calculation is 20 kHz and 2 kHz respectively. The position that the motor rotates during the sampling period ΔT_2 cause the maximum error in the estimated position. The maximum error is formulated as

$$\theta_{err} = \frac{P\omega\Delta T_2}{60} \times 360 \quad (7)$$

where ΔT_2 is the sampling period of the position estimator. The position error is about 1.8° and 9° from (7), as shown in Fig. 15(a) and (b), and the speed error is 6.944 rpm, that is the lowest recognizable speed. In practical, the three Hall sensor signals are first amplified by analog circuit. Therefore, the amplitude and DC offset of them may be different or with noise. Fig. 16 and 17 shows the position and speed estimation result when the Hall sensor signals are non-ideal. In Fig. 16(a), the amplitude of H_a and H_b are 102% and 98% of the idea value; In Fig. 16(b), the offset of H_a and H_b are 2% and -2% of the idea value. Fig. 17 shows the simulation result when there is 5% noise on three Hall signals. Due to that the estimated speed is the differential of the position, the speed estimated error is more obvious than the position error, and thus a low-pass filter is needed to reduce the error.

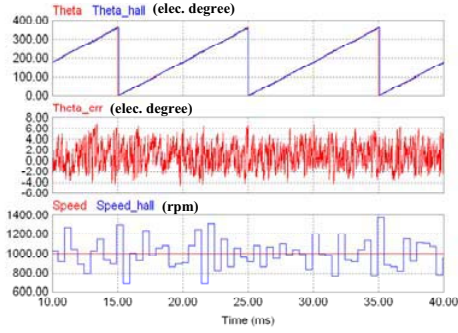


Fig. 17. Simulation results with 5% noise on Hall sensor signals.

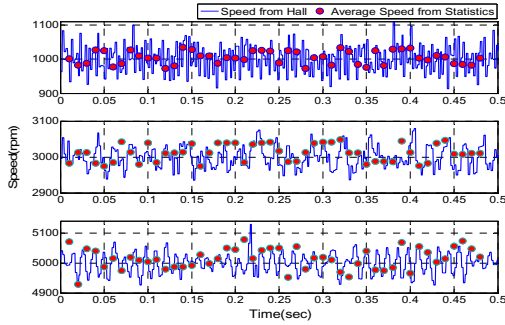


Fig. 18. Steady-state speed responses.

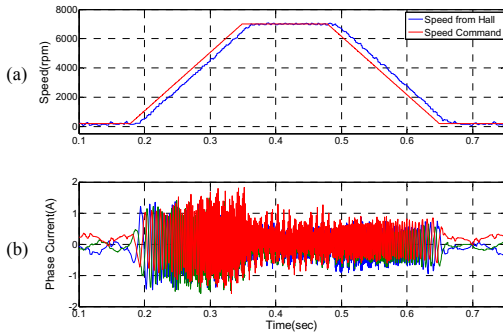


Fig. 19. Experimental results with Hall sensors under a ramping speed control. (a) ramping speed command and measured speed, (b) phase current responses.

IV. EXPERIMENTAL RESULTS

This PMSM servo control IC has been implemented employing the field programmable gate array (FPGA) technology by an Altera EP1C12F256C8, and the total logic cells are about 4237 of total 12060 (41%). The servo commands and the control parameters in this IC are configured via the serial communication port by a host PC. A program designed by GUI in Matlab is used for system constructors to setup the parameters in this IC.

To test the performance of the servo controller, a DVD spindle PMSM is used and the parameters are in Table I. In the experiment system, the PWM switching frequency is set at 20 kHz, and the sampling rate of the current loop and

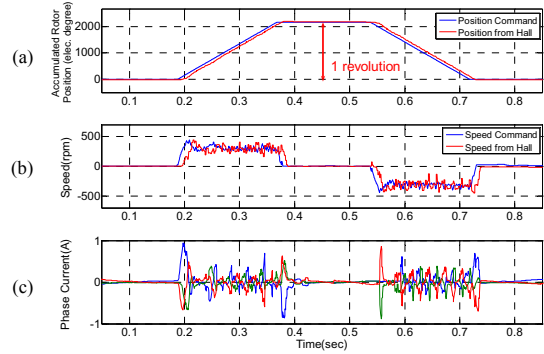


Fig. 20. Experimental results with Hall sensors under a ramping position control. (a) ramping position command and measured position, (b) speed command and estimated speed, and (c) phase current responses.

servo loop are 20 kHz and 2 kHz respectively. Fig. 18 shows the steady state speed response under speed command 1000, 3000 and 5000 rpm. The estimated speed is compared with the statistics of the average speed calculated from the average frequency of linear Hall sensor in a random period of time. Because the frequency of linear Hall sensor signals is proportional to the motor speed and calculating the frequency is less sensitive to the influence of noise, the speed derived from it is more approximate to the real motor speed. In Fig. 18, the speed ripple is about 70 rpm at low and high speed and the estimated result in the IC is quite similar to the average speed from statistics. Fig. 19 shows the speed response of a ramping speed control from 200 to 7000 rpm with the acceleration rate of 40 rpm per millisecond. Fig. 20 shows the position response under a ramping position control with the acceleration rate of 2 mechanical degrees per millisecond in one revolution. The position control resolution is 0.17 mechanical degree and the following error is about 16 mechanical degree. From this figure, quick transient response and accurate steady-state response can be achieved by using the proposed servo control IC.

V. CONCLUSION

This paper presents the design and implementation of a digital servo control IC for PMSMs with linear Hall sensors. All the control functions are realized by using digital reusable circuitry with a single-chip FPGA device, the Altera EP1C12F256C8. The total logic cells for the designed digital servo IC are about 4237 of total 12060 (41%) and this makes it suitable for low-cost CMOS ASIC implementation. This digital position control IC is configurable with its modular blocks and is programmable with its control registers via a serial interface to fit various applications without complicated software programming as realized by using conventional DSP or microcontrollers. The constructed servo control IC can achieve a control resolution of 0.17 mechanical degree, it also provides a simple and systematic solution for high-performance AC drives for small PMSM motors with linear Hall sensors.

TABLE I
PARAMETERS OF THE TESTED MOTOR

3-phase permanent magnet synchronous motor	
Type	Y-connection, 12 poles
Rated voltage	12 V
Stator resistance	0.5 Ω
Stator inductance	0.102 mH
Back-EMF constant	0.423 mV/rpm
Rotor inertia	1.056×10^{-6} kg \cdot m ²
Mech. time constant	0.27 sec

REFERENCES

- [1] T. M. Jahns, "Motion control with permanent-magnet AC machines," *IEEE Proc.*, vol. 82, no. 8, pp. 1241-1252, Aug. 1994.
- [2] Ying-Yu Tzou and Tien-Sung Kuo, "Design and implementation of an FPGA-based motor control IC for permanent magnet AC servo motors," *IEEE IECON Conf. Rec.*, vol. 2, pp. 943-947, Nov. 1997.
- [3] Kuang-Yao Cheng, Chen-Yu Wang, and Ying-Yu Tzou, "ASIC implementation of a programmable servo control IC with digital phase-locked loop," *IEEE PESC Conf. Rec.*, vol. 2, pp. 558-563, June 2002.
- [4] Zhaoyong Zhou, Tiejai Li, T. Takahashi, and E. Ho, "FPGA realization of a high-performance servo controller for PMSM," *IEEE APEC*, vol. 3, pp. 1604-1609, 2004.
- [5] Naizheng Cui, Guijie Yang, Yajing Liu, and Pinzhi Zhao, "Development of an FPGA-based high-performance servo drive system for PMSM," *IEEE ISSCAA*, pp. 881-886, Jan. 2006.
- [6] G. M. Raimondi, D. Howe, and P. H. Mellor, "Assessment of alternative current control methods for brushless permanent magnet motors," *PCIM Proc.*, pp. 133-140, Nurnberg, Germany, June 1997.
- [7] H. W. Park, S. J. Park, J. W. Ahn, Y. B. Choo, M. H. Lee, and C. U. Kim, "A novel optimal excitation scheme of brushless DC motor," *IEEE ISIE Conf. Rec.*, pp. 656-660, 1999.
- [8] F. Caricchi, F. Giulii Capponi, F. Crescimbin, and L. Solero, "Sinusoidal brushless drive with low-cost linear Hall effect position sensors," in *Proc. IEEE PESC Conf.*, vol. 2, pp. 799-804, June 2001.